Synthesis and Exceptional Operational Durability of Polyaniline-Inspired Conductive Ladder Polymers

Journal:	*Materials Horizons*
Manuscript ID	MH-COM-06-2023-000883.R1
Article Type:	Communication
Date Submitted by the Author:	04-Jul-2023
Complete List of Authors:	Leng, Mingwan; Texas A&M University Koripally, Nandu; University of California San Diego, Department of Electrical and Computer Engineering Huang, Junjie; Texas A&M University, Chemistry Vriza, Aikaterini; Argonne National Laboratory, CNM; Lee, Kyeong Yeon; Texas A&M University, Materials Science and Engineering Ji, Xiaozhou; Texas A&M University, Chemistry Li, Chenxuan; Texas A&M University, Chemistry Hays, Megan; Texas A&M University, Chemistry Tu, Qing; Texas A&M University System, Materials Science & Engineering; Dunbar, Kim R; Texas A&M University, Chemistry Xu, Jie; Argonne National Laboratory, CNM Ng, Tse Nga; University of California San Diego, Department of Electrical and Computer Engineering Fang, Lei; Texas A&M University, Chemistry; Texas A&M University, Materials Science and Engineering

SCHOLARONE™
Manuscripts

New Concept

This article introduces a new concept in the field of conductive polymers, through the development of low-defect ladder polymers inspired by polyaniline. Distinguished from existing research, this innovative approach utilizes a unique ladder-type molecular design strategy that results in an open-shell conductive polymer with exceptional robustness. Through a novel molecular design approach, we demonstrated that this ladder polymer exhibits intrinsic conductivity and unmatched resilience under harsh acidic or UV-irradiated conditions, and demonstrates robust performance across numerous redox cycles, notably surpassing commercial benchmarks. A further point of differentiation is the material's remarkable redox cyclability when used in operational electrochromic and supercapacitor devices. The insights gained from this study not only advance our mechanistic understanding of open-shell conductive polymers but also set a promising trajectory for the development of future generations of conductive polymers. This new concept has the potential to reshape the design of durable, high-performance redox-active organic electronic materials, paving the way for significant advancements in the fields of smart materials, energy storage, and bioelectronic interfaces.

Synthesis and Exceptional Operational Durability of Polyaniline-Inspired Conductive Ladder Polymers

Mingwan Leng[1], Nandu Koripally[3], Junjie Huang[1], Aikaterini Vriza[4], Kyeong Yeon Lee[2],

Xiaozhou Ji[1], Chenxuan Li[1], Megan Hays[1], Qing Tu[2], Kim Dunbar[1], Jie Xu[4]*, Tse Nga Ng[3]*,

and Lei Fang,[1,2]*

[1]   Department of Chemistry, Texas A&M University, College Station, TX 77843-3255, USA

[2]   Department of Materials Science and Engineering, Texas A&M University, College Station, TX 77843-3255, USA

[3]   Department of Electrical and Computer Engineering, University of California San Diego, La Jolla, California 92093, United States

[4]   Nanoscience and Technology Division, Argonne National Laboratory, Lemont, Illinois 60439, United States

* Email: xuj@anl.gov, tnn046@ucsd.edu, fang@chem.tamu.edu

Abstract:

Ladder-type structures can impart exceptional stability to polymeric electronic materials. This article introduces a new class of conductive polymers featuring a fully ladder-type backbone. A judicious molecular design strategy enables the synthesis of a low-defect ladder polymer, which can be efficiently oxidized and acid-doped to achieve its conductive state. The structural elucidation of this polymer and the characterization of its open-shell nature are facilitated with the assistance of studies on small molecular models. An autonomous robotic system is used to optimize the conductivity of the polymer thin film, achieving over 7 mS/cm. Impressively, this polymer demonstrates unparalleled stability in strong acid and under harsh UV-irradiation, significantly surpassing commercial benchmarks like PEDOT:PSS and polyaniline. Moreover, it displays superior durability across numerous redox cycles, performing exceptionally as the active material in an electrochromic device and as the pseudocapacitive material in a supercapacitor device. This work provides a structural design guidance for durable conductive polymers for long-term device operation.

Introduction

Conjugated ladder polymers represent a distinct class of macromolecules characterized by multiple strands of covalent bonds along a π-conjugated backbone. This unique constitution features an uninterrupted sequence of π-conjugated rings along the mainchain, with adjacent rings sharing at least two common atoms[1]. The fused, conjugated backbone often imparts conjugated ladder polymers with exceptional stability, even under extreme conditions and in operating devices[2-6]. In addition, the ladder-type constitution can offer advantages in electronic properties, because the

backbone rigidity lowers reorganization energy during charge transport while the coplanarity promotes delocalization of states.[7, 8] For instance, the ladder polymer poly(benzimidazobenzophenanthroline) (BBL) exhibits *n*-type electrical conductivity as high as 8 S cm^{-1} after doping,[9] *n*-type mobility[10] up to 1 cm^{2}V^{-1}s^{-1} on field effect transistors, and high geometry-normalized transconductance ($g_{m,norm} \approx 11$ S cm^{-1}) on electrochemical transistors.[11] In addition, BBL also boasts exceptional stability, which enables the processing of this material under strong acidic conditions[12] and ensures long-term durability of device performance without encapsulation or environmental control. We envision that the unique advantages offered by the ladder-type constitution could also be harnessed to enhance the stability and device performance of derivatives of polyaniline, which represents one of the most widely applied redox switchable conductive polymers.

Being redox active, highly conductive after doping[13], inexpensive, and easy to synthesize[14], oligoanilines and polyanilines have been utilized in a wide range of applications, such as in commercial products for antistatic coatings[15] and corrosion protection[15]. Moreover, it demonstrates significant potential as an active material for batteries[16-18], supercapacitors[19, 20], electrochromic devices[21, 22], and sensors[23, 24]. Polyaniline can undergo reversible redox reactions between the reduced leucoemeraldine base (LB) state, partially oxidized emeraldine base (EB) state, and fully oxidized pernigraniline base (PB) state. Acid doping of the EB and PB states gives the emeraldine salt (ES) and pernigraniline salt (PS) states, respectively. The ES state is known to be highly conductive. However, these acid doped states of polyaniline, especially the fully oxidized and protonated PS state, have limited stability.[25, 26] Previous research on the conductive nature of the PS state has been debated because the poor stability of the PS form hinders comprehensive investigation.[27, 28] Moreover, such poor stability impacts the long-term

performance of polyaniline-based devices, particularly those involving redox processes such as electrochromic or energy storage devices.[28]

In order to address the stability issue of polyaniline, we developed and investigated a class of ladder-type polyaniline analogues, *e.g.*, **f-LPANI** and **TolMSQ** shown in **Figure 1a**.[4, 29] Several significant findings were revealed. Firstly, the ladder polymer **f-LPANI** exhibited unprecedented stability even in the PS state. This high stability enabled an unambiguous demonstration of polaron delocalization in the fully oxidized and acid-doped PS state of **f-LPANI**, which exhibits Pauli Paramagnetism and electrical conductivity.[4, 29] More recently, single-molecule junction study on a similar small molecular model **TolMSQ** showed robust switching of the single-molecule conductance between the LB, PB, and PS states, among which the PS state exhibited the highest conductance.[30] These findings suggest that ladder-type polyaniline analogues, as a class of robust electronic materials with switchable properties, have highly promising application prospects. However, these applications still face a number of critical challenges. On one hand, although **f-LPANI** is intrinsically conductive in the PS state, its overall bulk conductivity in the thin film state is relatively low ($\sim 10^{-6}$ S cm^{-1}) due to the presence of a high content of nonconductive side chains (70.8 wt %) in its molecular structure. On the other hand, the basicity of **f-PANI** is comparatively weak, requiring a large amount of strong acid to dope the material into the conductive state. This requirement may lower device performance and introduce engineering challenges. To address these issues, we report herein the synthesis, mechanistic studies, and applications of a new type of polyaniline-inspired conjugated ladder polymers, **P1a** and **P1b**, along with their small molecular analogues, **1a~1c**. **P1a** not only exhibits conductivity that is four orders of magnitude higher compared to **f-LPANI**, but also displays a high doping efficiency. More importantly, **P1a** demonstrates remarkable durability in operating electrochromic and supercapacitor devices,

outperforming benchmark materials such as polyaniline and poly(3,4-ethylenedioxythiophene) polystyrene sulfonate (PEDOT:PSS).

Results and Discussion

In order to achieve a higher conductivity and ensure the desired excellent stability in ladder-type polyaniline analogues, we designed **P1a** (**Figure 1**) based on several key principles. First, the polymer should possess a well-defined, ladder-type structure with minimal structural defects. Potential defects of a ladder polymer backbone, such as uncyclized sites or regioisomerization, can arise due to low conversion or side reactions during the cyclization step[31]. Formation of defects should be prevented in order to avoid negative impacts on the stability and electronic properties of the resulting materials. Second, for efficient acid doping of the PB state into the conductive PS state, the PB backbone must be endowed with strong enough basicity to facilitate protonation with a minimum amount of acid. Finally, the content of insulating side-chain needs to be minimized while ensuring reasonable solubility and solution processability.
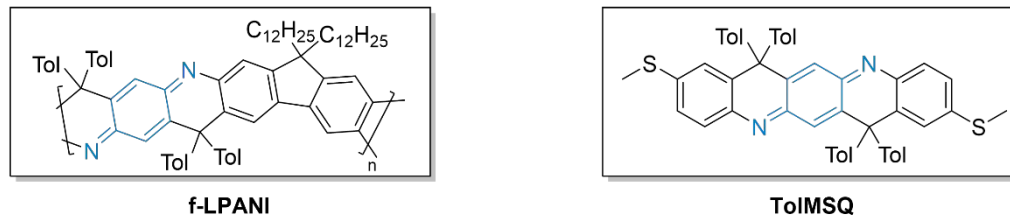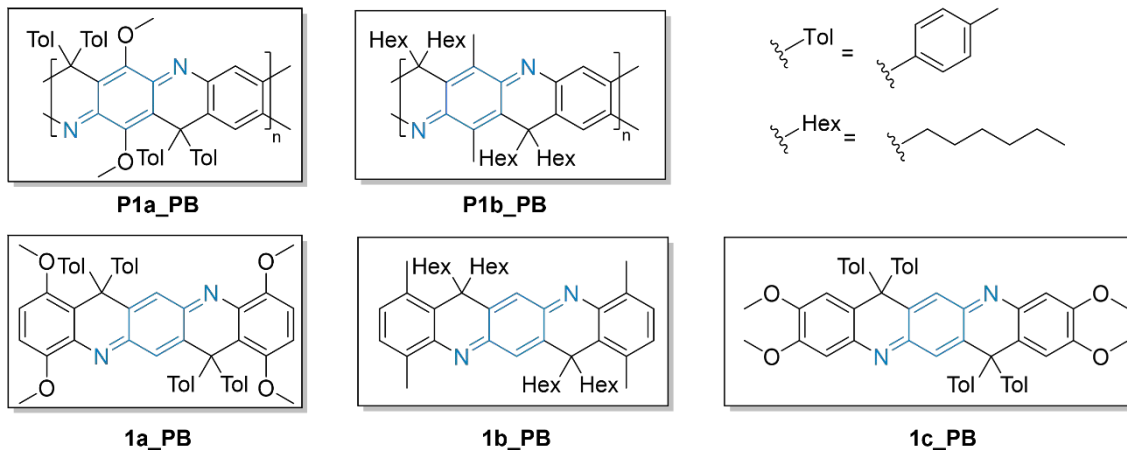
(a) Previous work:

f-LPANI

TolMSQ

(b) This work:

P1a_PB

P1b_PB
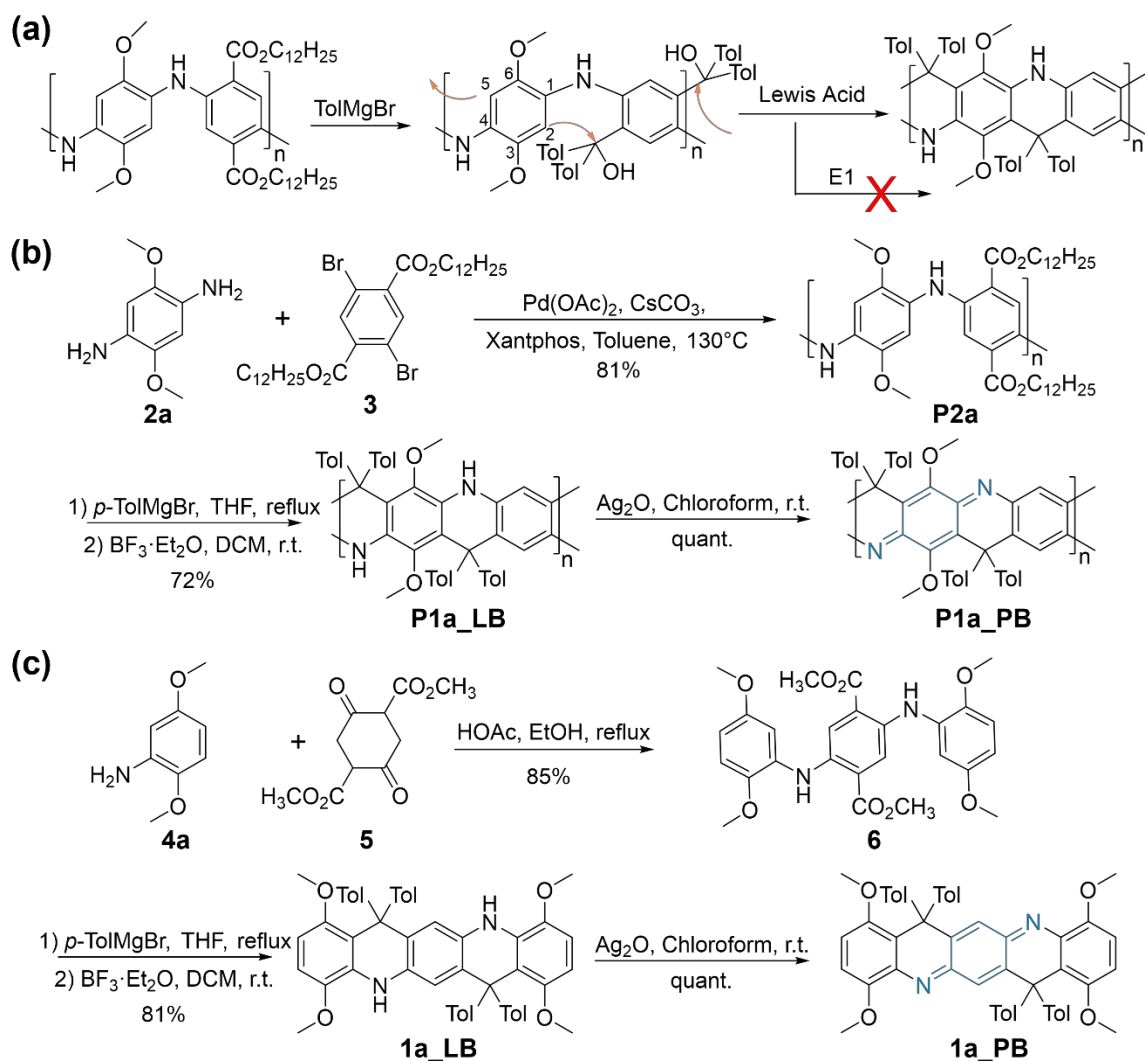

1a_PB

1b_PB

1c_PB

Figure 1. (a) Structural formulas of the previously reported ladder polymer **f-LPANI** and small molecule **TolMSQ**. (b) Structural formulas of ladder polymers **P1a** and **P1b**, as well as small molecule model compounds **1a, 1b,** and **1c**, all studied in this work. The suffix "**PB**" in these labels indicates that these structures are shown in the form of pernigraniline base.

In our designed strategy for synthesizing the ladder polymer **P1a**, the key cyclization step is an intramolecular Friedel-Crafts reaction between an electron-rich *p*-phenylene diamine unit and a tertiary alcohol function on a neighboring unit (**Scheme 1a**). In order to promote the electrophilic aromatic cyclization only at the 2,5 positions of the *p*-phenylene diamine unit while avoiding the formation of undesired regioisomers, we installed two methoxy side groups on the 3- and 6-positions. These electron-donating methoxy groups can (*i*) block the 3- and 6-positions hence prevent the formation of undesired isomers, (*ii*) increase the nucleophilicity of the phenylene

diamine unit to promote the electrophilic aromatic cyclization reaction, and (*iii*) enhance the basicity of the product, allowing more efficient acid doping. To ensure the solubility along the synthesis and processability of the final product, the bridge sp^3 carbons of **P1a** were decorated by solubilizing groups, which can be installed during the step of Grignard reaction. It is important to note that undesired E1 elimination can take place during the subsequent Lewis acid-promoted cyclization step. Thereby, a solubilizing group without hydrogen β to the hydroxyl group was desired to avoid potential defects along the backbone caused by such E1 elimination. In this context, tolyl magnesium bromide was used to install the bridge carbon. On parallel, a similar polymer **P1b** with less electron-rich methyl groups installed on the 3,6-positions was designed as a control for direct comparisons. Three small molecular analogues, namely, **1a, 1b,** and **1c** were also designed and synthesized as models to better characterize and understand the properties of the polymeric samples.

The synthesis of **P1a** started with the Buchwald-Hartwig cross-coupling polymerization between diamino-functionalized monomer **2a** and dibromo-diester-functionalized monomer **3** (**Scheme 1b**). The resulting polyaniline-like intermediate **P2a** (M_n = 12.6 kg mol^{-1}, $Đ$ = 2.02) was obtained in good yield and exhibited good solubility thanks to the presence of the long C_{12} chain attached to the ester functionalities. Subsequently, **P2a** was treated by *p*-tolyl magnesium bromide to convert the carboxylic ester groups into tertiary alcohol groups, followed by cyclization promoted by BF$_3$, to afford the ladder-type polymer product **P1a** in its LB form (**P1a_LB**) (M_n = 11.2 kg mol^{-1}, $Đ$ = 2.0). The conditions for the Grignard and cyclization reactions were optimized to minimize the possibility of unreacted defect sites. Meanwhile, the absence of β-hydrogen on the tolyl group precludes potential elimination side-reactions involving the tertiary alcohol group during the Lewis acidic cyclization reaction. Consequently, the final conjugated ladder polymer, **P1a_LB**, was

obtained without any observable defects (see **SI**). The oxidized form of the polymer (**P1a_PB**) ($M_n = 11.8$ kg mol^{-1}, $Đ = 1.91$) was obtained in a quantitative conversion by treating **P1a_LB** with Ag$_2$O. The control polymer **P1b** was synthesized using a similar method (**Scheme S11**), yielding **P1b_PB** with an M_n of 20.3 kg mol^{-1} and a $Đ$ of 1.73.

Scheme 1. (a) Key steps during the synthesis: Grignard reaction to generate the tertiary alcohol groups followed by Lewis acid catalyzed intramolecular Friedel-Crafts cyclization. (b) Synthesis of **P1a_LB** and **P1a_PB**. (c) Synthesis of **1a_LB** and **1a_PB.**

The synthesis of the small molecular model **1a** began with an imine condensation reaction between amino-functionalized starting material **4a** and dimethylsuccinylsuccinate **5**.[32, 33] The resulting intermediate **1a** was subsequently subjected to reaction conditions similar to the synthesis of **P1a**, to afford **1a_LB** and **1a_PB** in high yields. Model compounds **1b** and **1c** were synthesized via similar procedures (see **SI**). These small molecular model compounds were fully characterized by using high-resolution mass spectrometry (HRMS), ^{1}H, ^{13}C, HSQC, and HMBC NMR spectroscopy (**Figure S27-34, 40-47**). The NMR peak assignments of these small molecular models were used as references to validate the NMR characterization and to assign the NMR peaks of polymer products **P1a** and **P1b** (**Figure S39**).

The ladder-type polyaniline analogues **P1a** and **P1b** were anticipated to undergo transformations between the LB, PB, and PS forms, in which the core phenylene-diamine unit was anticipated to interconvert between aromatic, closed-shell quinoidal, and open-shell states, respectively (**Figure 2a**). The difference in these forms, thereby, can be characterized by difference in the bond lengths of the phenylene-diamine unit. In order to do so, we attempted the growth of single crystals of the small molecular model compounds. Fortunately, single crystal structures of the LB form of **1a**, the PB form of **1b**, and the PS form of **1c** were successfully obtained (see details in **SI**). Despite the difference of the peripheral functional groups of these model compounds, the backbones share the same constitution so that the bond length comparison of these crystal structures offer a good structural comparison of these three different states (**Figure 2b**). In our comparison, five bonds in the core phenylene-diamine moiety were labeled from *a~e*. The aromatic **1a_LB** showed small bond length alternation (BLA). Specifically, *b, c,* and *d* are nearly equal at the value of a typical benzene ring (*b*: 1.395 Å, *c*: 1.390 Å, *d*: 1.396 Å), confirming the aromatic nature of the ring in the LB state. Meanwhile, the bond lengths of *a* (1.396 Å) and *e* (1.391 Å) represented the typical

lengths of a C—N single bond. In contrast, the crystal structure of **1b_PB** exhibited the largest

BLA. Bond lengths of *b* (1.449 Å) and *d* (1.453 Å) became close to that of a single bond, while

bond *c* (1.351 Å) was much shorter like a double bond. Bonds *a* (1.303 Å) and *e* (1.303 Å) were

close to the length of C=N double bonds. Finally, in **1c_PS**, the protonated PS state exhibited a

medium BLA due to the contribution of both quinoidal and aromatic resonance forms. Bonds *b*

(1.417 Å) and *d* (1.411 Å) were shorter than single bonds, but longer than bonds in benzene rings,

while bond *c* (1.371 Å) was longer than a double bond and shorter than bonds in benzene rings.

The lengths of bonds *a* and *e* (both 1.353 Å) were also between the length of a C—N single bonds

and a double bond. The BLA values of the **1c_PS** suggested a partially open-shell nature. Based

on this structure, DFT calculation and natural orbital analysis of **1c_PS** was performed, revealing

a diradical character of 0.57 (**Figure S6**). These data on small molecular models give us a

quantitative analogy of the aromatic, quinoidal, and open-shell natures of the various redox and

protonation states of the polyaniline-analogous ladder polymers **P1a** and **P1b**.

We tested the redox transformation and recyclability of **P1a** between the LB and PB forms.

Starting from **P1a_LB**, the addition of an oxidant reagent (*m*-CPBA) to its THF solution led to the

conversion to **P1a_PB**, accompanied by a distinct color change from pale yellow to green and then

to blue. This color change was recorded by UV-vis absorption spectroscopy to show the

appearance of a peak around 650 nm and the decrease of the UV-absorption band with a clear

isosbectic point (**Figure S1**). Upon the subsequent addition of a reducing reagent,

diethylhydroxylamine, the solution reverted to its original pale-yellow color via an intermediate

green state. The UV-vis absorption spectrum was also restored to the original state. The

electrochemical interconversion was also investigated via cyclic voltammetry (CV) analysis

(**Figure S8-9**). In the presence of proton acid or lithium ion, recyclable electrochemical

transformation between the oxidized and reduced forms were observed, which has also been observed on small molecule models **1a** (**Figure S7**) and **1b** (**Figure S10**). Electrochemical oxidation without acid in $TBAPF_6$ electrolyte was also performed to measure the HOMO level of the ladder polymers in their PB states. The HOMO levels were measured to be −5.03 eV for **P1a_PB** (with $-OCH_3$ side chains) (**Figure S8**) and −5.65 eV for **P1b_PB** (**Figure S11**) (with $-CH_3$ side chains). Similarly, **1a_LB** (-4.50 eV, **Figure S7**) was also measured to have higher HOMO than **1b_LB** (-4.90 eV, **Figure S10**). The significantly higher HOMO of **P1a_PB** demonstrated the strong impact of the methoxy groups on enhancing the electron density of the ladder polymer backbone.
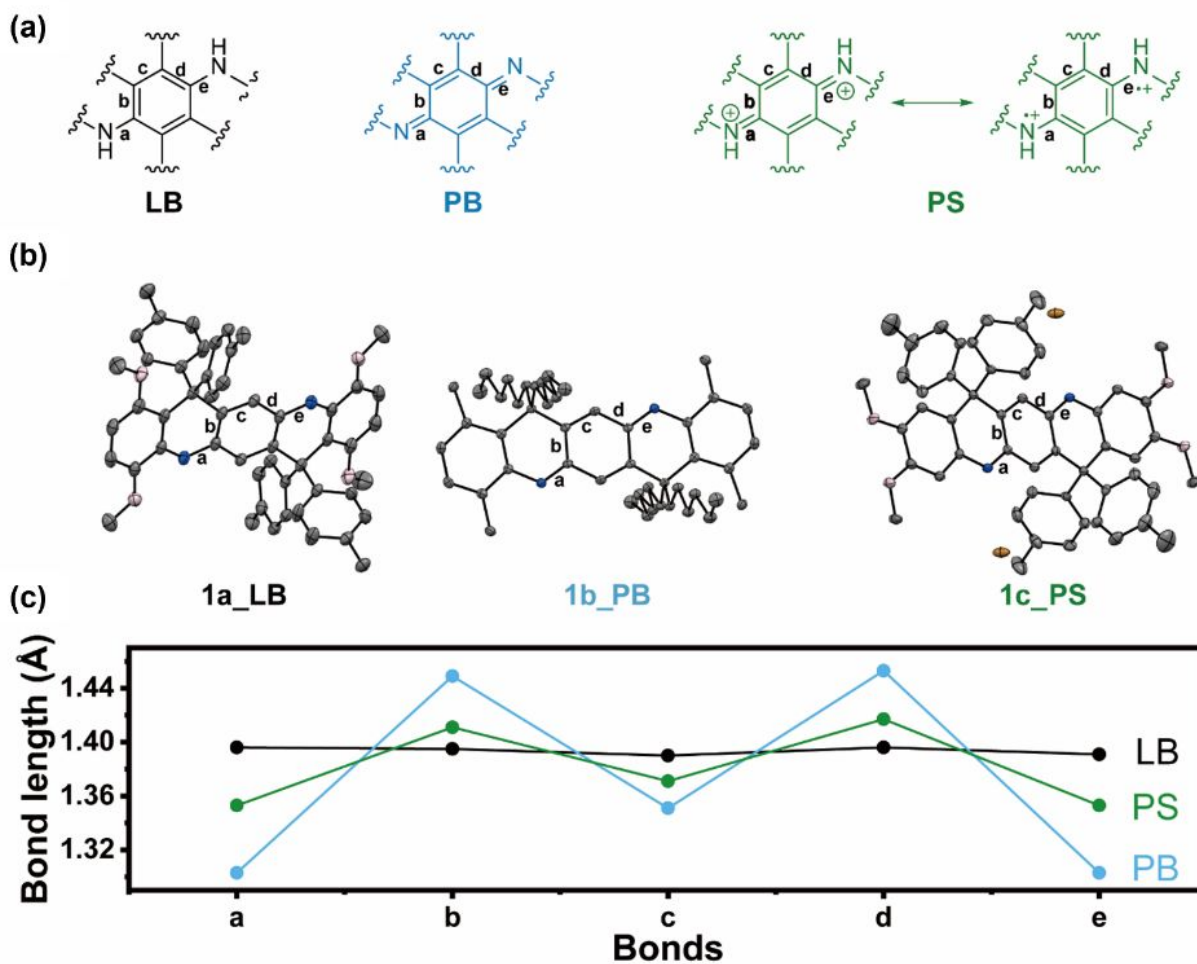

Figure 2. (a) Structures and bond labeling of the LB, PB and PS forms; (b) Single-crystal structures

of **1a_LB, 1b_PB,** and **1c_PS**. Hydrogen atoms and solvent molecules are omitted for clarity.

Thermal ellipsoids are scaled to the 50% probability level. (c) Comparison of bonds lengths of the

phenylene diamine core, marked as a, b, c, d and e.

Given its electron-rich nature, **P1a_PB** was anticipated to be protonated more easily than the less electron-rich control polymer **P1b_PB**. The acid titration process of both polymers (concentration counting on repeating unit $= 1 \times 10^{-4}$ mol L^{-1}) with methanesulfonic acid (MSA) was monitored using UV-visible-near infrared absorption spectroscopy in a THF solution (**Figure 3**). The addition of MSA into **P1a_PB** resulted in the emergence of a low energy near infrared absorption peak ($\lambda_{max} \sim 1000$ nm; $\lambda_{onset} \sim 1600$ nm) and diminishing of the original absorption band ($\lambda_{max} \sim 620$ nm), while presenting a distinct isosbestic point. The low energy absorption peak signifies the characteristic formation of the PS state. Despite multiple protonation stages in **P1a_PB**, the clear isosbestic point indicated a distinct transformation from the unprotonated state to the doubly protonated state for each repeating unit at the concentration used in this titration experiment. The concentrations of unprotonated **P1a_PB** and fully protonated **P1a_PS** were plotted as a function of MSA concentration[34] (**Figure 3a**, right). Full protonation was nearly accomplished when the MSA concentration reached 250 mmol L^{-1}. In stark contrast, **P1b_PB,** with less electron-rich methyl substituents, was much harder to protonate. A model study on small molecule **1b_PB** showed that it could only be mono-protonated although there were two basic sites on the molecule (see **Figure S2**). The same was observed for **P1b_PB**, where each repeating unit could only be mono-protonated to give **P1b_PB·nH^{n+},** even if the concentration of MSA reached 250 mmol L^{-1} (**Figure 3b)**. The fully protonated state of **P1b_PS** could not be achieved within a reasonable acid concentration. Among these two polymers, the higher basicity and feasible protonation process of **P1a_PB** enabled its application as a conductive polymer with acid doping.
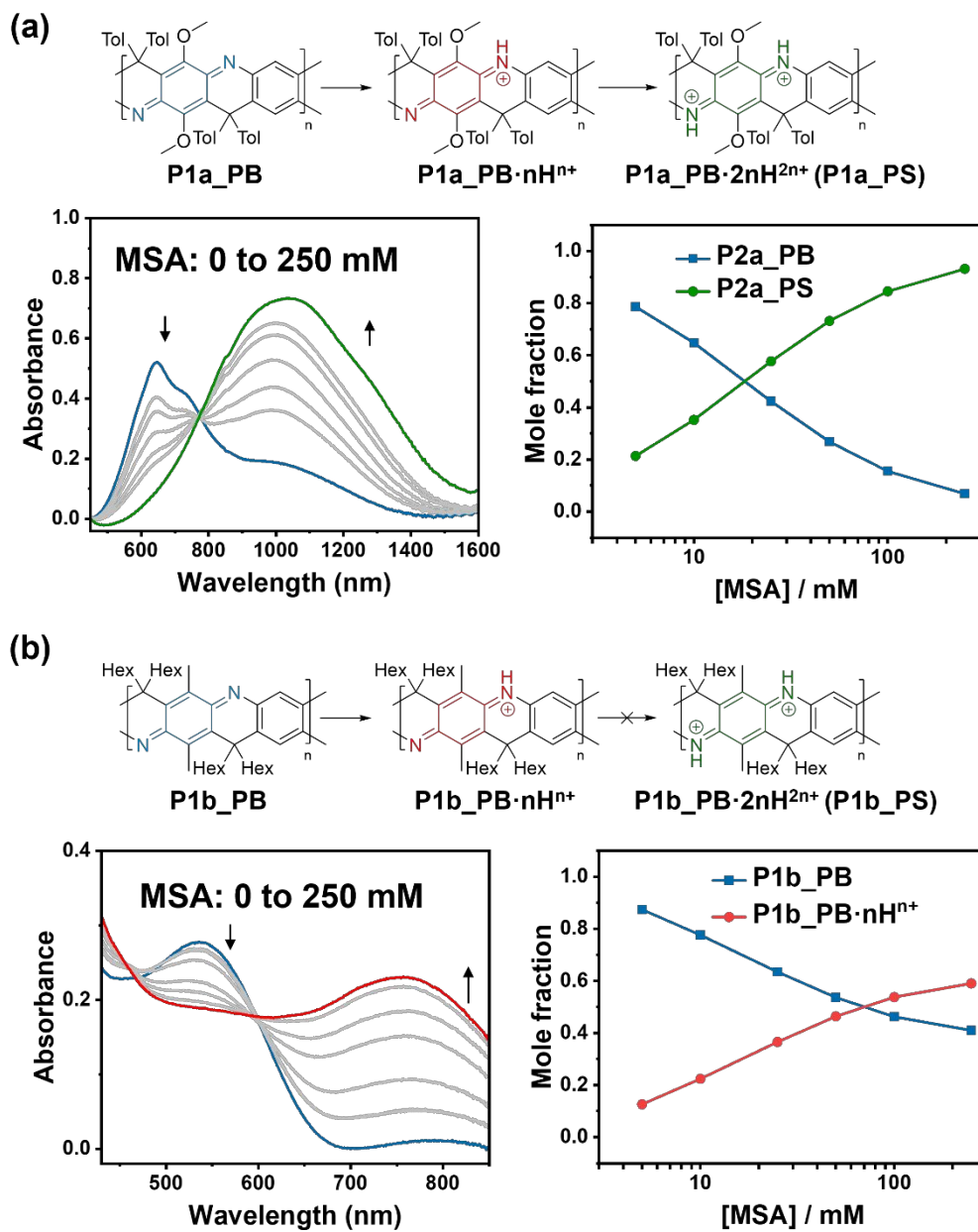
Figure 3. UV-vis-NIR absorption spectra (left) and molar fraction calculated using Bind-fit (right) corresponding to doping process of (a) **P1a_PB** (concentration of repeating unit: 1×10^{-4} mol L^{-1}) and (b) **P1b_PB** (concentration of repeating unit: 1×10^{-4} mol L^{-1}) with increasing amount of MSA.

Upon full protonation, the PS form of the ladder type polyaniline analogues are anticipated to be partially open-shell as indicated by the crystal structure of **1c_PS**.[4, 29] The open-shell nature of

P1a_PS and **1a_PS** was validated by electron paramagnetic resonance (EPR) spectroscopy in solid state. The solid samples were prepared by mixing **P1a_PB** or **1a_PB** mixed with 2 equivalents of *p*-Toluenesulfonic acid (PTSA). EPR spectra of both samples (**Figure S3**) showed broad and strong one-line signal (*g* factors = 2.0010-2.0030), confirming their open-shell character and the presence of radical cations (polarons) in the solid state. The nature of these polarons were further investigated by using a variable temperature superconducting quantum interference device (SQUID) from 2 K (**Figure S5**). The results showed that both **P1a_PS** and **1a_PS** had a triplet ground state (S = 1) with a small positive coupling constant ($J = 0.5$ cm^{-1} for **P1a_PS** and 0.12 cm^{-1} for **1a_PS**), suggesting weak ferromagnetic coupling between the radical pair. This coupling is possibly facilitated by the rigidity and coplanarity of the conjugated ladder-type backbone. Both **P1a_PS** and **1a_PS** displayed temperature-independent Pauli paramagnetism (**Figure 4a**) at 4×10^{-3} and 1×10^{-2} emu per mole of repeating unit, indicating a delocalized nature of the radical cations (polarons). Compared to that of polyaniline[35] ($\chi_{Pauli} \sim 10^{-4}$ emu per mole of repeating unit), both **P1a_PS** and **1a_PS** exhibited higher χ_{Pauli}, suggesting a stronger delocalization effect of the polarons in the solid state. This observation agreed well with that observed previously on **f-LPANI** oligomers[29]. Among these two, the higher χ_{Pauli} of **P1a_PS** suggested that longer ladder polymer chains enable the extension of polaron delocalization, likely through an intrachain mechanism. In sharp contrast, the solid-state mixture of **P1b_PB** and **1b_PB** with large excessive of PTSA (10 equivalent) remained diamagnetic because they could not be fully acid-doped due to low basicity (**Figure S4**).

The presence of delocalized polarons in **P1a_PS** suggests that they are electrically conductive. Initial conductivity measurements were conducted on a sample prepared from mixing **P1a_PB** with 1 equivalent of PTSA. The mixture was pressed into a pellet and a 4-point probe conductivity

measurement gave a conductivity of 1.10×10^{-3} S cm^{-1} at ambient conditions. This value was already 10^3 times higher than that measured on **f-LPANI**, likely due to the lower content of insulating side chains in **P1a** (58.2% wt), as compared with that of **f-LPANI** (70.8%). To further explore the doping formula and testing conditions for achieving high conductivity of **P1a_PS** in the thin film state, an automated solution processing and characterization systemin the self-driving laboratory named Polybot was employed[36]. This platform comprises an enclosed frame with a N_2 environment, liquid and substrate/vials handling system, coating station with programmable speed, annealing stage, electronic characterization systems and on-line data analysis. Various films of acid-doped **P1a_PS** were coated on SiO_2 substrates for quick screening. The electronic conductivities were measured by Keithley 4200 using the 4-point probe method. The sequence of automated operations includes i) solution formulation, ii) coating, iii) annealing, and iv) 4-point probe measurements of conductivity (**Figure 4b**). We investigated a two-dimensional experimental space to dope **P1a_PB** comprising of the following parameters: acid type (Lewis and proton acids) and concentration (equivalents). A total of 12 distinct types of acids and 10 different concentrations (equivalents from 1 to 10) were treated as categorical variables. To facilitate the exploration of this experimental space, we employed the Latin Hypercube Sampling (LHS) to allow for comprehensive and uniform sampling across the entire parameter space.[37] During the thin film preparation and characterization process, Polybot system tested all the parameters proposed by LHS and created a series of thin films with measured conductivities. The experimental points explored are presented in **Figure 4c** where grey circles represent all the possible experimental space. A localized optimum is observed for high equivalents for HCl. The conductivity reached 7×10^{-3} S cm^{-1}, which is much higher than the initial value measured.
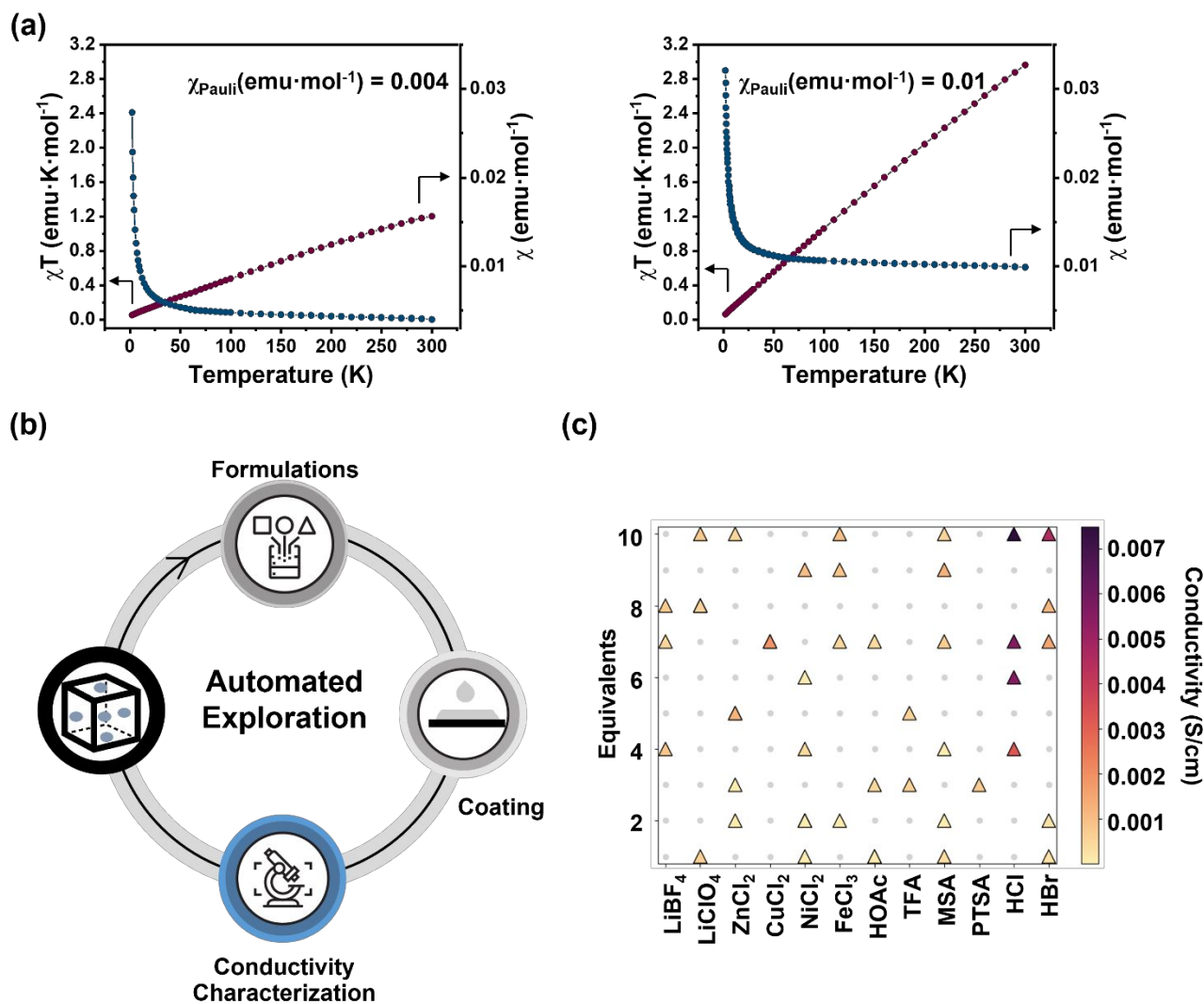
Figure 4. (a) Temperature-varied magnetic susceptibility of 2 equivalents PTSA mixed **1a_PS** (left) and **1a_PS** (right); (b) Workflow of the automated conductivity screening by Polybot; (c) Plot of conductivity data points measured by Polybot.

As a conjugated ladder polymer, **P1a** was anticipated to possess high durability against harsh conditions. Here, we studied not only the stability of **P1a** in acidic conditions but also under strong UV irradiation. The acid stability of **P1a** or other polyaniline analogues is important, as these types of materials often need to function in acidic conditions to achieve their conductivity and redox

switchability.[32, 33] Firstly, **P1a_PS** was dissolved in the strong acid MSA, and the absorption spectrum was monitored using UV-vis-NIR spectroscopy. Remarkably, little change was observed on its spectrum even after 16 days (**Figure S12**). In comparison, the benchmark commercial conductive polymer, PEDOT:PSS[38-41], tested in the same conditions, showed decomposition within a few days, as evidenced by a drastic change of the absorption spectrum in the 300-800 nm range. Likewise, commercial polyaniline exhibited a fast decomposition within hours and fully decomposed after one week when dissolved in MSA, due to the dissociation of imine bond in strong acidic conditions.[42-44] UV light is also known to be extremely aggressive for organic materials.[45-47] Here the photostability of **P1a_PS** (prepared from drop-casting a solution of **P1a_PB** with 4 equivalents of PTSA in THF) and control polymers in a thin film state was examined when exposed to UV light (Intensity: 10 mW cm^{-2}) (**Figure 5**). To ensure that the absorbance wavelength of all the polymers was covered, both 254 nm and 365 nm wavelength UV lamps were used simultaneously. After 8 hours, the absorbance of the **P1a_PS** film did not show any obvious change (**Figure 5a**). In comparison, the absorbance of a PEDOT:PSS film decreased for 50% after 8 hours, which is attributed to the morphological change or light induced oxidation, as mechanism study proposed in literature (**Figure 5b**).[48-50] When PEDOT:PSS was mixed with PTSA, it was even more vulnerable under UV irradiation, exhibiting quicker decomposition within 3 hours (**Figure 5c**). The exceptional photostability of **P1a_PS** is unmatched by non-ladder type conductive polymers, and was only observed on other ladder polymers such as BBL derivatives.[51, 52] This result provides a solid foundation for the use of conductive ladder polymers in real-world applications where UV irradiation is inevitable, such as in outdoor wearable devices. The photostability will also enable this conductive ladder polymer to withstand harsh processing conditions, such as those involving UV-crosslinking or curing.
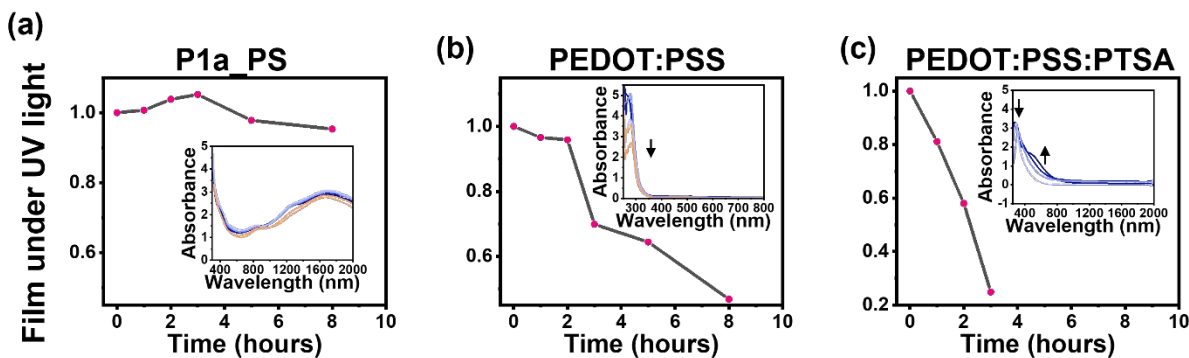
Figure 5. Plots of UV-vis-NIR absorbance intensity at λ_{max} as a function of time under 254 nm and 365 nm UV irradiation (10 mW cm^{-1}): (a) **P1a_PB** + 4 equivalents of PTSA (**P1a_PS**); (b) PEDOT:PSS; and (c) PEDOT:PSS + 4 equivalents of PTSA film. The insets are the corresponding UV−vis-NIR absorption spectra over time.

The outstanding stability, robust redox transformation, and good conductivity of **P1a** make it a highly promising active material for electrochemical device applications.[22] We further investigated the performance durability of **P1a** in operating electrochromic and energy storage devices. **P1a_PB** was applied as the active material in a sandwiched electrochromic device, which was composed of two ITO–glass substrates, a spin-cast **P1a_PB** thin film, and a layer of lithium gel electrolyte (PMMA/PC/LiClO$_4$). Under a +2 V positive bias (oxidative potential on the active layer), the active layer turned into deep blue and exhibited a NIR absorption feature with λ_{max} = 900 nm according to the spectroelectrochemical measurement (**Figure S13**). This color change was a result of the formation of **P1a_PS** with the Li$^+$ doping from the electrolyte layer. Upon switching the bias to −2 V, the device exhibited a pale yellowish-green color as a result of electrochemically reducing **P1a_PS** into **P1a_LB**. The device was cycled between −2V/+2V repeatedly, and the color change was measured each time. After 200 cycles, the color change exhibited only less than 5% degradation, showing excellent robustness and recyclability between

this wide voltage window. In fact, the slight degradation after 200 cycles was on account of the exfoliation of the **P1a** layer from the glass substrate due to the mechanical brittleness of the film, not a result of intrinsic chemical decomposition. In comparison, a similar electrochromic device fabricated with PEDOT: PSS showed significant degradation after only 20 cycles under the same test conditions (**Figure S14**).
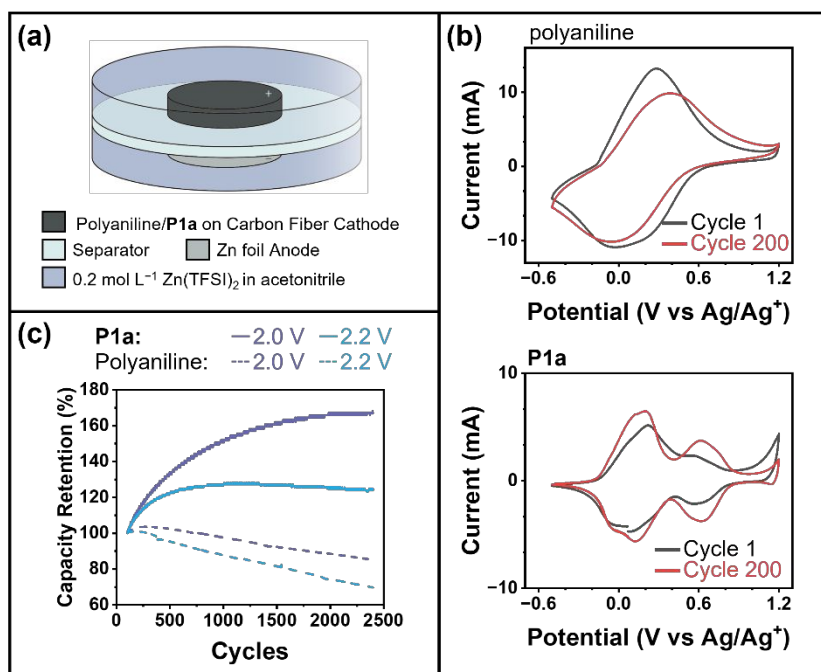

Figure 6. (a) Setup of supercapacitor for measurements. (b) 3-electrode cyclic voltammetry (CV) of polyaniline and **P1a** over a 1.7 V window. (c) Plot of capacity against number of cycles of 2-electrode polyaniline and **P1a** devices over a 0.2 ~ 2V and 0.2 ~ 2.2V range, respectively.

Polyaniline has been widely employed as the pseudocapacitive electrode materials for supercapacitors, thanks to its redox activity and conductivity.[19, 53, 54] However, these devices often show a drastic performance decline over charge/discharge cycles.[55-58] As a more stable analogue of polyaniline, **P1a** is anticipated to also function as pseudocapacitive electrode material, while offering much better durability during device operation.[59]

We fabricated coin cell supercapacitors[60-62] by using either polyaniline or **P1a**, by drop casting the active material onto carbon cloth to reach a 0.5 mg loading (**Figure 6a**). This electrode was used as the cathode, and the anode was a 100 μm thick Zn foil. The separator was a glass microfiber with a thickness of 260 μm. The electrolyte was a acetonitrile solution of $Zn(TFSI)_2$ ($0.2mol\ L^{-1}$). First, we investigated the redox durability of polyaniline and **P1a** using a 3-electrode configuration. An Ag/AgCl reference electrode was inserted in the electrolyte, and the measurements were taken in an inert N_2 atmosphere in a glovebox. Cyclic voltammetry scans of polyaniline and **P1a** were recorded at 100 mV s^{-1} in the 3-electrode setup by sweeping the cell from −0.5 to 1.2V (**Figure 6b**). The current of the polyaniline electrode decreased over 200 cycles, and the shift in the redox peaks indicated that the reaction was not fully reversible at this 1.7 V window. In contrast, **P1a** showed no decrease but an increase in current after 200 cycles, and the symmetric redox peaks indicated an excellent reversibility of the redox reactions after these repeated cycles.[63]

Stability and galvanostatic charge-discharge (GCD) measurements were taken on these supercapacitor cells in ambient conditions with a 2-electrode setup. The sealed coin cells prevented the evaporation of the electrolyte solvent acetonitrile and allowed for longer cycling than the 3-electrode setup. The coin cells were cycled from 0.2 to 2.0 or 2.2V for 2400 cycles at 4 A g^{-1}. The capacity of the polyaniline coin cells peaked around 200 cycles and then dropped by 8% and 31% after 2400 cycles for the 2 V and 2.2 V ranges, respectively. In contrast, the capacity of the **P1a** coin cells increased and stabilized over time (**Figure 6c**). The cycling was stopped at 2400 cycles due to limitation of the Zn anode, in which dendritic formations on the Zn anode started to penetrate the separator and short circuited the cell[64]. No decline of the cell capacity was observed at the point of 2400 cycles. The individual GCD curves are presented in **Figure S15**. The decreased capacity of polyaniline is indicated by the shorter charge-discharge period at the 2400th cycle. In

contrast, **P1a** shows the opposite characteristics with an increased charge-discharge period at the end of cycling, so its percentage retention of capacity became over 100% compared with beginning. This rise in capacity is associated with expansion and contraction of polymers with cycling which made the film morphology more accommodating to counter ion movement and increase the cell capacity. In this study, although the observed current output and capacity of the **P1a** electrode were lower than that of polyaniline due to the presence of inert solubilizing groups that curtailed the theoretical capacitance, this limitation can be addressed by changing the design and synthesis of ladder polyaniline analogues with side chains of low molecular weights, considering that solubility of the material for supercapacitor application is not strictly required. Importantly, our findings validate the premise that ladder-type polyaniline analogues, as presented in this study, can operate within a considerably broader potential range, and demonstrate superior redox stability in supercapacitor devices compared to commercial polyaniline.

Conclusions

In conclusion, this work showcases the design and synthesis of an exceptionally durable conductive polymer, **P1a**. The strategic molecular design enabled us to achieve a low-defect ladder polymer structure and facilitate efficient acid doping of the product. Through studies on small molecular models, magnetic characterization, and optimization of conductivity, we elucidated the open-shell, conductive nature of the pernigraniline salt form of the polymer (**P1a_PS**). Remarkably, **P1a_PS** not only demonstrated stability under harsh acidic or UV-irradiated conditions, but also exhibited robust redox transformations over a large number of cycles in operational electrochromic and supercapacitor devices. The insights gained from this study pave the way for future developments of truly stable, high-performance, redox-active organic electronic materials. Such materials are poised to be highly desirable in various devices, including supercapacitors, electrochromic devices, and electrochemical transistors. Nonetheless, overcoming the challenges associated with multi-step synthesis from non-commercial starting materials remains a prerequisite for these materials to significantly propel advancements in crucial fields like smart materials, energy storage, and bioelectronic interfaces.

References

1.   A. D. Jenkins, P. Kratochvíl, R. F. T. Stepto and U. W. Suter, *Pure Appl. Chem.*, 1996, **68**, 2287-2311.
2.   K. Yu, X. Ji, T. Yuan, Y. Cheng, J. Li, X. Hu, Z. Liu, X. Zhou and L. Fang, *Adv. Mater.*, 2021, **33**, 2104558.
3.   G. Ma, M. Leng, S. Li, Z. Cao, Y. Cao, D. P. Tabor, L. Fang and X. Gu, *J. Mater. Chem. C*, 2022, **10**, 13896-13904.
4.   X. Ji, M. Leng, H. Xie, C. Wang, K. R. Dunbar, Y. Zou and L. Fang, *Chem. Sci.*, 2020, **11**, 12737-12745.
5.   C. Zhu, A. J. Kalin and L. Fang, *Acc. Chem. Res.*, 2019, **52**, 1089-1100.
6.   J. Wu, X. Rui, C. Wang, W.-B. Pei, R. Lau, Q. Yan and Q. Zhang, *Adv. Energy Mater.*, 2015, **5**, 1402189.
7.   S. Che, J. Pang, A. J. Kalin, C. Wang, X. Ji, J. Lee, D. Cole, J.-L. Li, X. Tu, Q. Zhang, H.-C. Zhou and L. Fang, *ACS Mater. Lett.*, 2020, **2**, 49-54.
8.   C. Zhu, X. Ji, D. You, T. L. Chen, A. U. Mu, K. P. Barker, L. M. Klivansky, Y. Liu and L. Fang, *J. Am. Chem. Soc.*, 2018, **140**, 18173-18182.
9.   C.-Y. Yang, M.-A. Stoeckel, T.-P. Ruoko, H.-Y. Wu, X. Liu, N. B. Kolhe, Z. Wu, Y. Puttisong, C. Musumeci, M. Massetti, H. Sun, K. Xu, D. Tu, W. M. Chen, H. Y. Woo, M. Fahlman, S. A. Jenekhe, M. Berggren and S. Fabiano, *Nat. Commun.*, 2021, **12**, 2354.
10. A. Babel and S. A. Jenekhe, *Adv. Mater.*, 2002, **14**, 371-374.
11. H.-Y. Wu, C.-Y. Yang, Q. Li, N. B. Kolhe, X. Strakosas, M.-A. Stoeckel, Z. Wu, W. Jin, M. Savvakis, R. Kroon, D. Tu, H. Y. Woo, M. Berggren, S. A. Jenekhe and S. Fabiano, *Adv. Mater.*, 2022, **34**, 2106235.
12. M. Leng and L. Fang, in *Ladder Polymers*, 2023, DOI: https://doi.org/10.1002/9783527833306.ch4, pp. 97-120.
13. Y. Wang, H. D. Tran, L. Liao, X. Duan and R. B. Kaner, *J. Am. Chem. Soc.*, 2010, **132**, 10365-10373.
14. J. Huang and R. B. Kaner, *J. Am. Chem. Soc.*, 2004, **126**, 851-855.
15. A. Zhu, H. Wang, S. Sun and C. Zhang, *Prog. Org. Coat.*, 2018, **122**, 270-279.
16. A. Mirmohseni and R. Solhjo, *Eur. Polym. J.*, 2003, **39**, 219-223.
17. P. Jiménez, E. Levillain, O. Alévêque, D. Guyomard, B. Lestriez and J. Gaubicher, *Angew. Chem. Int. Ed.*, 2017, **56**, 1553-1556.
18. S. Chen, K. Li, K. S. Hui and J. Zhang, *Adv. Funct. Mater.*, 2020, **30**, 2003890.
19. A. Eftekhari, L. Li and Y. Yang, *J. Power Sources*, 2017, **347**, 86-107.
20. F. Ran, Y. Tan, W. Dong, Z. Liu, L. Kong and L. Kang, *Polym. Adv. Technol.*, 2018, **29**, 1697-1705.
21. L. Zhao, L. Zhao, Y. Xu, T. Qiu, L. Zhi and G. Shi, *Electrochim. Acta*, 2009, **55**, 491-497.
22. M. Almtiri, T. J. Dowell, I. Chu, D. O. Wipf and C. N. Scott, *ACS Appl. Polym. Mater.*, 2021, **3**, 2988-2997.
23. S. Virji, J. Huang, R. B. Kaner and B. H. Weiller, *Nano Lett.*, 2004, **4**, 491-496.

24.   J. Huang, S. Virji, B. H. Weiller and R. B. Kaner, *Chemistry–A European Journal*, 2004, **10**, 1314-1319.
25.   L. D. Arsov, W. Plieth and G. Koßmehl, *J. Solid State Electrochem.*, 1998, **2**, 355-361.
26.   R. Mažeikien and A. Malinauskas, *Eur. Polym. J.*, 2002, **38**, 1947-1952.
27.   G. D'Aprano, M. Leclerc and G. Zotti, *Macromolecules*, 1992, **25**, 2145-2150.
28.   F. F. C. Bazito, L. T. Silveira, R. M. Torresi and S. I. Córdoba de Torresi, *Phys. Chem. Chem. Phys.*, 2008, **10**, 1457-1462.
29.   X. Ji, H. Xie, C. Zhu, Y. Zou, A. U. Mu, M. Al-Hashimi, K. R. Dunbar and L. Fang, *J. Am. Chem. Soc.*, 2020, **142**, 641-648.
30.   J. Li, B.-J. Peng, S. Li, D. P. Tabor, L. Fang and C. M. Schroeder, *Chem*, DOI: 10.1016/j.chempr.2023.05.001.
31.   J. Lee, A. J. Kalin, T. Yuan, M. Al-Hashimi and L. Fang, *Chem. Sci.*, 2017, **8**, 2503-2521.
32.   Y. Zou, T. Yuan, H. Yao, D. J. Frazier, D. J. Stanton, H.-J. Sue and L. Fang, *Org. Lett.*, 2015, **17**, 3146-3149.
33.   Y. Zou, X. Ji, J. Cai, T. Yuan, D. J. Stanton, Y.-H. Lin, M. Naraghi and L. Fang, *Chem*, 2017, **2**, 139-152.
34.   P. Thordarson, *Chem. Soc. Rev.*, 2011, **40**, 1305-1323.
35.   V. I. Krinichnyi, A. L. Konkin and A. P. Monkman, *Synth. Met.*, 2012, **162**, 1147-1155.
36.   A. Vriza, H. Chan and J. Xu, *Chem. Mater.*, 2023, **35**, 3046-3056.
37.   M. D. McKay, R. J. Beckman and W. J. Conover, *Technometrics*, 2000, **42**, 55-61.
38.   S.-M. Kim, C.-H. Kim, Y. Kim, N. Kim, W.-J. Lee, E.-H. Lee, D. Kim, S. Park, K. Lee, J. Rivnay and M.-H. Yoon, *Nat. Commun.*, 2018, **9**, 3858.
39.   A. M. Nardes, M. Kemerink, M. M. de Kok, E. Vinken, K. Maturova and R. A. J. Janssen, *Org. Electron.*, 2008, **9**, 727-734.
40.   E. Vitoratos, S. Sakkopoulos, E. Dalas, N. Paliatsas, D. Karageorgopoulos, F. Petraki, S. Kennou and S. A. Choulis, *Org. Electron.*, 2009, **10**, 61-66.
41.   A. Elschner, *Sol. Energy Mater. Sol. Cells*, 2011, **95**, 1333-1338.
42.   F. R. Simões, L. A. Pocrifka, L. F. Q. P. Marchesi and E. C. Pereira, *The Journal of Physical Chemistry B*, 2011, **115**, 11092-11097.
43.   O. E. Bogomolova and V. G. Sergeyev, *The Journal of Physical Chemistry A*, 2018, **122**, 461-469.
44.   A. G. MacDiarmid, S. K. Manohar, J. G. Masters, Y. Sun, H. Weiss and A. J. Epstein, *Synth. Met.*, 1991, **41**, 621-626.
45.   A. Tournebize, J.-L. Gardette, C. Taviot-Guého, D. Bégué, M. A. Arnaud, C. Dagron-Lartigau, H. Medlej, R. C. Hiorns, S. Beaupré and M. Leclerc, *Polym. Degrad. Stab.*, 2015, **112**, 175-184.
46.   M. Imran, C. M. Wehrmann and M. S. Chen, *J. Am. Chem. Soc.*, 2019, **142**, 38-43.
47.   Z. Peeters, O. Botta, S. B. Charnley, Z. Kisiel, Y.-J. Kuan and P. Ehrenfreund, *A&A*, 2005, **433**, 583-590.
48.   P. Tehrani, A. Kanciurzewska, X. Crispin, N. D. Robinson, M. Fahlman and M. Berggren, *Solid State Ion.*, 2007, **177**, 3521-3527.
49.   D.-J. Yun, J. Jung, Y. M. Sung, H. Ra, J.-M. Kim, J. Chung, S. Y. Kim, Y.-S. Kim, S. Heo, K.-H. Kim, Y. J. Jeong and J. Jang, *Advanced Electronic Materials*, 2020, **6**, 2000620.
50.   Y. Wu, S. S. Nagane, P. Sitarik, S. Chhatre, J. Lee and D. C. Martin, *J. Mater. Chem. A*, 2022, **10**, 8440-8458.

51.   Y. Zhang, L. Chen, K. Zhang, H. Wang and Y. Xiao, *Chemistry – A European Journal*, 2014, **20**, 10170-10178.
52.   F. Coter, Y. Belaish, D. Davidov, L. R. Dalton, E. Ehrenfreund, M. R. McLean and H. S. Nalwa, *Synth. Met.*, 1989, **29**, 471-476.
53.   K. Zhang, L. L. Zhang, X. S. Zhao and J. Wu, *Chem. Mater.*, 2010, **22**, 1392-1401.
54.   X. Chang, Z. Yang, A. Huang, Y. Katsuyama, C.-W. Lin, M. F. El-Kady, C. Wang and R. B. Kaner, *Macromol. Rapid Commun.*, 2023, e2300237-e2300237.
55.   T. Liu, L. Finn, M. Yu, H. Wang, T. Zhai, X. Lu, Y. Tong and Y. Li, *Nano Lett.*, 2014, **14**, 2522-2527.
56.   Y. He, X. Wang, H. Huang, P. Zhang, B. Chen and Z. Guo, *Appl. Surf. Sci.*, 2019, **469**, 446-455.
57.   J. Yang, X. Yu, X. Sun, Q. Kang, L. Zhu, G. Qin, A. Zhou, G. Sun and Q. Chen, *ACS Appl. Mater. Interfaces*, 2020, **12**, 9736-9745.
58.   Y. Lin, H. Zhang, W. Deng, D. Zhang, N. Li, Q. Wu and C. He, *J. Power Sources*, 2018, **384**, 278-286.
59.   M. Almtiri, T. J. Dowell, H. Giri, D. O. Wipf and C. N. Scott, *ACS Appl. Polym. Mater.*, 2022, **4**, 3088-3097.
60.   C. Shin, L. Yao, H. Lin, P. Liu and T. N. Ng, *ACS Energy Lett.*, 2023, **8**, 1911-1918.
61.   L. Yao, J. Liu, N. Eedugurala, P. Mahalingavelar, D. J. Adams, K. Wang, K. S. Mayer, J. D. Azoulay and T. N. Ng, *Cell Rep. Phys. Sci.*, 2022, **3**, 100792.
62.   K. Wang, L. Yao, M. Jahon, J. Liu, M. Gonzalez, P. Liu, V. Leung, X. Zhang and T. N. Ng, *ACS Energy Lett.*, 2020, **5**, 3276-3284.
63.   H. K. Bok and S. M. Oh, *J. Electrochem. Soc.*, 2008, **155**, A685.
64.   W. Nie, H. Cheng, Q. Sun, S. Liang, X. Lu, B. Lu and J. Zhou, *Small Methods*, **2023**, 2201572.